

Model-based inference of a directed network of circadian neurons

Journal Title
XX(X):1-11
©The Author(s) 2018
Reprints and permission:
sagepub.co.uk/journalsPermissions.nav
DOI: 10.1177/ToBeAssigned
www.sagepub.com/



David McBride^{1,2}, Linda Petzold^{1,2}

Abstract

The suprachiasmatic nucleus (SCN) is the master clock of the brain. It is a network of neurons that behave like biological oscillators, capable of synchronizing and maintaining daily rhythms. The detailed structure of this network is still unknown, and the role that the connectivity pattern plays in the network's ability to generate robust oscillations has yet to be fully elucidated. In recent work, we used an information theory-based technique to infer the structure of the functional network for synchronization, from bioluminescence reporter data. Here, we propose a computational method to determine the directionality of the connections between the neurons. We find that most SCN neurons have a similar number of incoming connections, but the number of outgoing connections per neuron varies widely, with the most highly connected neurons residing preferentially in the core.

Keywords

Circadian, Suprachiasmatic Nucleus, Network, Inference, Computational

Introduction

A majority of living organisms display internal rhythms that oscillate with nearly 24 hour periods. These are called circadian rhythms and control gene expression in cells, as well as bodily processes and behavioral patterns in larger organisms Dunlap (1999). The main pacemaker for this process in mammals is the suprachiasmatic nucleus (SCN), a neuronal network comprised of approximately 20,000 neurons, situated in the ventral hypothalamus Ralph et al (1990). This neuron cluster acts to entrain the body's circadian rhythms with environmental light/dark cycles, as well as to subsequently entrain peripheral physiological functions Bass and Takahashi (2010). While individual cells within this network display circadian oscillations, the robust system properties and stability necessary to be useful in a dynamic biological system do not emerge without communication between the individual oscillators Liu et al. (2007), Stelling et al. (2004). The cells communicate and synchronize via neurotransmitters and neuropeptides. The transcription-translation feedback loop that produces oscillations within a single cell has been extensively studied and modeled Leloup and Goldbeter (2003), To et al. (2007). However, the network dynamics are dependent on the topology of the SCN network as a whole.

Much work has been done to elucidate the mechanisms of communication in the SCN Aton et al. (2005), DeWoskin et al. (2015). The main mechanism focused on in this paper is signaling via vasoactive intestinal polypeptide (VIP) to achieve synchronization of the clock protein PERIOD2 (PER2) via CREB (cAMP response element-binding protein) and the resulting synchronization of PER2 expression among cells in the SCN. Additional work has been conducted to explore the nature of the network structure. Several potential topologies have been examined Cutler et al. (2003),

Vasalou et al. (2009), including nearest neighbor, Strogatz-Watts, and exponential networks. Some models Gonze et al. (2005) have also used a mean-field mechanism to attain synchrony in the system. Data analysis techniques applied to PER expression data using a bioluminescent reporter have suggested that a small world network with an exponentially distributed node degree provides a good fit to observed network properties Abel et al. (2016). This type of network is also consistent with what is known about the development of neurons and their structure Cutler et al. (2003). There are several modes of coupling amongst neurons in the brain. These include synaptic connections, gap junctions, and diffusing signals. Mechanisms such as diffusing signals do not exhibit directionality, as they are diffusion mediated and so transmitters simply move along concentration gradients. Gap junctions more directly connect two cells, and allow for rapid transmission of electrical signals and exchange of small molecules. This direct connection goes both ways, and therefore does not exhibit directionality. Connections between the axons and dendrites, however, may exhibit directionality. While it is possible for a neuron to both send a signal to another neuron via its axons as well as receive that second neuron's signals at its own dendrites, it is not a requirement. It is possible for a neuron to only receive a signal in this manner, or only send it. Thus, neural connections give rise to networks that are partially, though not exclusively, directed. Recent research has focused on which cells were connected, but not on the directionality

¹University of California, Santa Barbara

²Institute for Collaborative Biotechnologies

Corresponding author:

Linda Petzold, Department of Computer Science University of California
2104 Harold Frank Hall Santa Barbara, California, 93106-5110

Email: petzold@engineering.ucsb.edu

of those connections. Since neurons do not necessarily communicate bi-directionally, to further understand these complex biological networks it is important that we know not only whether or not two cells are connected, but also whether the signal goes from cell A to cell B or vice versa.

Other works [Abrahamson and Moore \(2001\)](#) have suggested an asymmetric distribution of nodes, with findings that indicate two distinct regions in the SCN lobes: a core and a shell. These works have found that the core is the main driver of synchrony [Welsh et al. \(1995\)](#), leading the PER oscillations while the shell lags slightly behind. Previous studies [Abel et al. \(2016\)](#) of the network connections of the SCN have also observed a higher number of connections within and extending from the core region. Furthermore, it is established [Cagampang et al \(1998\)](#) that while a majority of neurons in the SCN, and nearly all in the shell [Kalamatianos et al. \(2004\)](#) are capable of receiving vasoactive intestinal polypeptide (VIP), the putative coupling agent for synchronization [Abel et al. \(2016\)](#), only approximately 20% are able to synthesize it [Kalamatianos et al. \(2004\)](#).

Functional network structures for neurons have been identified using techniques including mutual information, transfer entropy, directed transfer functions, Granger causality, and between-sample analysis of connectivity (BSAC) [Abel et al. \(2016\)](#), [Garofalo et al. \(2009\)](#), [Bettencourt et al. \(2007\)](#), [Kaminski et al. \(2001\)](#), [Pourzanjani et al. \(2015\)](#), [Fujita et al. \(2010\)](#). However, each of these methods has one of two issues. They are either inappropriate for determining the directionality of connections, or the lack of high frequency data and slow nature of the feedback loop controlling the core SCN oscillator render the technique not applicable. For example, high-frequency GABA signals affect the firing of SCN neurons and have been mapped previously [Garofalo et al. \(2009\)](#); however, fast scale GABA is not thought to affect the core oscillator [DeWoskin et al. \(2015\)](#), but rather it is primarily driven by slow-scale VIP, resulting in the damping of high-frequency signals [Fujita et al. \(2010\)](#), [Webb et al. \(2012\)](#). Additionally, while the maximal information coefficient (MIC) has been used to identify the functional connectivity of the SCN [Abrahamson and Moore \(2001\)](#), it does not provide information regarding the directionality of those connections.

This paper makes two primary research contributions. First, we introduce a model-based methodology for inference of directionality of network connections. Second, we apply this methodology to infer the directionality of four networks of SCN cells. By analyzing the resynchronization data from four mouse SCN explants with knock-in PERIOD2:Luciferase, we confirm that there are likely phase-leading nodes that entrain others, and that these nodes reside preferentially in the core. We find that the SCN forms a directed network with an exponentially distributed outgoing node degree, but a normally distributed incoming node degree. This further supports the idea that driver nodes are the primary controllers of the SCN phase. Based on these findings, we suggest that this structure serves a purpose of balancing the ability of the system to synchronize and re-entrain quickly with the ability to maintain robust oscillations that are not desynchronized by short time scale perturbations.

Methodology and results

Data gathering

To collect the data for this experiment, four mouse SCNs were sliced and cultured under a microscope. Images were captured every hour and tracking software [Abel et al. \(2016\)](#) was used to identify and ascribe bioluminescence values to individual cells. The complete methodology is detailed in the "Biological Methods" section of [Abel et al. \(2016\)](#). Tetrodotoxin (TTX), a neurotoxin that inhibits intercellular signaling, was applied and left for six days. The TTX was then washed from the system and the subsequent resynchronization was observed for eight days. The hourly data from the resynchronization portion of these experiments was then used to infer the network structure. The full dataset used to obtain results is publicly available online at <https://github.com/JohnAbel/scn-resynchronization-data-2016>.

Inference of directed connections between SCN neurons

Basic concept

The basic concept for our method is as follows: given the data, which consists of PER2 concentrations at 60 minute intervals, and a simple model (we use a phase-amplitude model from [Garofalo et al. \(2009\)](#)), minimize the difference between the data and the model predictions as a function of the directionality of the network connections between each pair of neurons. Thus, we have

$$\min(C) \sum \|PER2_{t,i} - \widehat{PER2}_{t,i}(C)\| \quad (1)$$

where C is the directed connectivity matrix and $PER2_{t,i}$ is the observed value of PER2 at time t for cell i . $\widehat{PER2}_{t,i}(C)$ is the model-predicted value of PER2 at time t for cell i , and is a function of the connections into cell i . The norm used is the L^2 norm.

The naive approach requires that we explore an exponentially increasing number of network configurations to be explored, needing to explore as many as 2^n possible network structures, where n is the number of nodes, and run full simulations for each of them. This rapidly becomes infeasible for large systems. For our networks of over 400 neurons, it would have taken more than a year to run all of the necessary simulations on a single processor machine.

Instead, we propose a method that solves a least squares problem, minimizing over the possible connection directionalities while constraining the weights for each connection to between 0 and 1. We begin by noting that the derivative of the phase of an oscillating system is given by the Velocity Response Curve (VRC) [Garofalo et al. \(2009\)](#), [Taylor et al. \(2010\)](#), which is a cell-specific function of the current phase and amplitude, and of the incoming VIP to each cell, which depends on the network connections, including their directionality. Using a forward Euler method to obtain the phase at time $t + 1$, given the phase at time t , we obtain

$$\phi_{i,t+1} = \phi_{i,t} + \Delta t(1 + VRC(\phi_{i,t}, A_{i,t})) \frac{VIP_{in,i}(t, C)}{VIP_{in,i}(t, C) + 12}. \quad (2)$$

The new phase, given by the model, can be expressed as a linear function of the connectivity matrix. Then, we minimize the error between the observed phase and the model predicted phase over the connections

$$\min(C) \sum \|\phi_i - \hat{\phi}_i(C)\| \quad (3)$$

Noting that, by multiplying through in equation 3 by the denominator of the fraction, it is easy to see that the new phase, given by the discretized model, can be expressed as a linear function of the connectivity matrix. Thus this minimization can be performed very efficiently via a linear least squares solver.

In our specific implementation we instead solved for VIP as a function of phase, and minimized the difference between predicted and observed incoming VIP, again leading to a linear least squares problem. A detailed description may be found in the Supplemental materials section.

It is important to note that there are two possible ways in which the model can come into the optimization. One could solve the ODE numerically, over the entire interval, and minimize, over all possible connectivities, the distance between the solution to this ODE and the data. Or, one could re-initialize the ODE at each data point, using the data. This introduces a complication, though, in that the phase-amplitude model will need initial values at each time point for both phase and amplitude, and both of these values will need to be determined from the PER2 data. We found that the second method, despite the complications of generating the required the initial values from the data, was much more robust.

In our inference of directionality, we began with the functional networks inferred in [Abel et al. \(2016\)](#).

Model

This inference approach requires a model that, given the data at time t and a proposed connectivity matrix C , can produce an approximation to the PER2 concentration at time $t + 1$. Due to the fact that the data gathered was limited to bioluminescent reporting of PER2, it seemed most appropriate to use the simple phase-amplitude model as established in [Taylor et al. \(2017\)](#) for the inference. The two differential equations that govern each neuron in the model are given by

$$\frac{d\phi_i(t)}{dt} = 1 + VRC(\phi_i(t), A_i(t), ss_i, \tau_i) \frac{\gamma_i(t)}{\gamma_i(t) + K}, \quad (4)$$

$$\frac{dA_i(t)}{dt} = -\lambda(A_i(t) - ss_i) + \kappa \frac{\gamma_i(t)}{\gamma_i(t) + K}, \quad (5)$$

where $\phi_i(t)$ is the phase of cell i , 1 represents the basal rate of phase change per hour (for an oscillator with a period of approximately 24 hours), $VRC(\phi_i(t), A_i(t), ss_i, \tau_i)$ represents the Velocity Response Curve (VRC) as a function of the phase, amplitude, steady state amplitude and period of the cell, respectively, $\gamma_i(t)$ is the incoming concentration of VIP averaged across inputs, and K is an activation threshold. Additionally, κ is the maximum growth rate of the amplitude, and λ is the decay rate. The VRC for each cell was determined using the equation

$$\exp \beta (ss_i - A_i(t)) VRC_{intrinsic}(\phi_i(t), ss_i, \tau_i), \quad (6)$$

where β is a parameter that scales the size of the VRC depending on the cell amplitude, ss_i is the uncoupled amplitude of the cell, and $VRC_{intrinsic}$ is an empirical curve shown in [Webb et al. \(2012\)](#) that gives a baseline VRC for all cells. This equation makes it so that higher amplitude cells respond less strongly to incoming signals.

The key feature of this model that allows it to work with our limited data comes from the fact that the PER concentration in each cell can be represented as an oscillator with a varying phase and amplitude, making it useful for predicting circadian behavior. Thus, the PER data can be converted into a series of phases and amplitudes for each cell and the response of the oscillators to external stimuli (VIP) can be modeled using velocity response curves (VRCs). The process for the conversion is outlined later in this Section.

The relaxation rate used in this model is $\lambda = 0.39 hr^{-1}$. This value is comparable to values examined in [Abraham et al. \(2010\)](#). It is within their definition of a rigid oscillator, which rapidly proceeds to its limit cycle state, but is still shown to produce a distribution of individual oscillators that are entrained to within approximately two hours of the system phase. When testing synthetic networks, values for ss_i were chosen from a normal distribution about 1 a.u. (arbitrary units) with a standard deviation of 0.2 a.u., similar to simulations in [Abraham et al. \(2010\)](#) and [Schmal et al. \(2018\)](#). With amplitude expansion, this resulted in an amplitude distribution with a mean of 5.5 a.u. and a standard deviation of 1.23 at limit-cycle amplitudes. The observed amplitude expansion in our simulations is similar to the approximately 5 fold increase found in experimental data in [Schmal et al. \(2018\)](#) for systems considered to have moderate coupling strength.

One caveat is that the specific model chosen likely affects the results. To be a candidate model for analyzing connection directionality, a model must have both a way to relate phase to neurotransmitter release and a relationship for how neurotransmitter inputs affect phase velocity. The model used in this paper has both. A family of VRCs tuned for this system is used to relate VIP input to phase change, and the model includes a prediction of VIP release based on a cells phase. Changing these factors will have the largest effect on the results.

Generation of phase and amplitude from the data

To use the phase-amplitude model to make predictions and infer network structure, it was necessary to obtain the phases and amplitudes from the PER2 data at each time point. To accomplish this, we made initial predictions of the phase and amplitude using the model, and refined the predictions via a minimization with regularization, as described below.

The phase values at peaks and troughs, as well as the amplitude values at peaks, were directly calculated. These points will henceforth be referred to as anchor points. Initial guesses for the remaining phases and amplitudes were generated assuming that each cell experiences a mean field concentration of VIP stimulus, and Euler's method was used to generate values from one anchor point to the next. A detailed explanation can be found in Supplement S1.

The initial guess for a time series between two anchor points was then refined by minimizing the l_2 -norm of the residuals of the difference between the model-generated concentration and the PER2 data for each time point according to:

$$\begin{aligned} \min_{\phi_{t,i}, A_{t,i}} \sum_t \gamma_1 \|PER2_{t,i} - \widehat{PER2}_{t,i}(\phi_{t,i}, A_{t,i})\| \\ + \gamma_2 \left\| \phi_{t,i} - \phi_{t-1,i} - t \frac{d\phi_{t-1,i}}{dt} \right\| \quad (7) \\ + \gamma_3 \left\| A_{t,i} - A_{t-1,i} - t \frac{dA_{t-1,i}}{dt} \right\|, \end{aligned}$$

where $\frac{d\phi_{t-1,i}}{dt}$ and $\frac{dA_{t-1,i}}{dt}$ are calculated according to equations 4 and 5, and γ_1 , γ_2 and γ_3 determine the relative importance of the model fit, the phase regularization and the amplitude regularization respectively.

The first regularization prevents the phase from deviating too much from the model inferred value. This keeps the phase within reasonable bounds from one time step to the next (i.e., no jumps from $\frac{\pi}{2}$ to $\frac{5\pi}{2}$). The second regularization prevents extreme amplitude changes by penalizing deviations away from the amplitude of the previous time step plus an expected deviation dependent on the mean VIP in the system. The phase and amplitude values found using this method were then used to solve for the incoming VIP_{in} .

Results

The method was tested using synthetic networks generated in silico. Directed networks were randomly generated, and the reduced model was used to produce a corresponding set of resynchronization data. The method described above was then used on this test data, given an undirected version of the network, to determine the success rate of the method. The parameters used to produce the test data were varied from those assumed during the inference, to test the robustness of the method. Additionally, Gaussian noise with a standard deviation of up to 50% of the mean amplitude of the oscillations was added to the synthetic data to test its effect on the accuracy of the inference. The results of the inference were evaluated for accuracy (ACC), sensitivity (TPR), and specificity (SPC) according to

$$ACC = \frac{TP + TN}{TP + TN + FP + FN} \quad (8)$$

$$TPR = \frac{TP}{TP + FN} \quad (9)$$

$$SPC = \frac{TN}{TN + FP}, \quad (10)$$

where TP is the number of true positives, TN is the number of true negatives, FP is the number of false positives and FN is the number of false negatives.

With Gaussian noise of 20% of the value of the mean amplitude applied, the inference of connections in the synthetic networks had an ACC of 82.6%, with a TPR of 88.5% and an SPC of 78.6%. With 10% noise those values become a 91.1% ACC, a 93.4% TPR, and an 88.2% SPC. When the anchor points were not used and the phase and amplitude values for the entire time series were determined

using only the initial conditions, the robustness of the method greatly decreased. The results of all of the trials are summarized in the Supplemental material.

Initial results from Abel et al. (2016) suggested that exploring the functional connectivity within SCNs revealed networks with an exponential node degree. Our work further supports this, finding an exponential node degree for outgoing connections. However, we also observe a truncated normally distributed node degree for incoming connections. This result illuminates previous experimental research that found that only approximately 20 percent of cells in the SCN express VIP Kalamatianos et al. (2004), while almost all SCN cells express the surface protein responsible for the detection of VIP. It seems likely that the highly connected nodes are VIP-ergic cells that drive the synchronization and entrainment of the system.

Over 99% of identified SCN neurons were determined to have three or fewer incoming connections. In contrast, approximately 80% of SCN neurons have three or fewer outgoing connections, while the remaining 20% are relatively highly connected nodes of outgoing degree 4 or larger. Among all cells, 60% have no outgoing connections at all. This suggests that most cells have some input from 1-3 other nodes, while approximately 20% of the cells are generating that input.

Discussion

In this work we have introduced a methodology for model-based inference of network directionality, and then used it to infer the directionality of the functional networks for synchronization of SCN slices. In this paper we sought the functional network structure for synchronization, which occurs on a relatively long timescale and is known to be driven mainly by neuropeptide mediated communication. We note that this is different from short time scale communication, which is important for other SCN functions, such as the electrical coupling used for visual function in Schmal et al. (2018).

The inference methodology is based on minimization of the difference between simple, local models and the data, over the time intervals for which the data was measured. Although we had data for only one chemical species: PER2 concentration, we showed how to make use of another optimization to obtain estimated time course information for both period and phase. The inference was then carried out simply and efficiently by solving a linear least squares problem. We anticipate that our overall approach may be extended to inference of directionality of more complex, multivariable problems where data is available for only some of the state variables, but strong correlations exist between the known and unknown variables.

In Abel et al., potential connections were identified between cells based on their phase progression as synchrony was restored to a system that had been disrupted with TTX. In this paper, we use those identified connections as the basis of our network, and then use a model to determine their direction. The directionality of the functional network for synchronization that we inferred from the slices revealed an asymmetric network where most neurons had an incoming node degree less than or equal to three, and the network

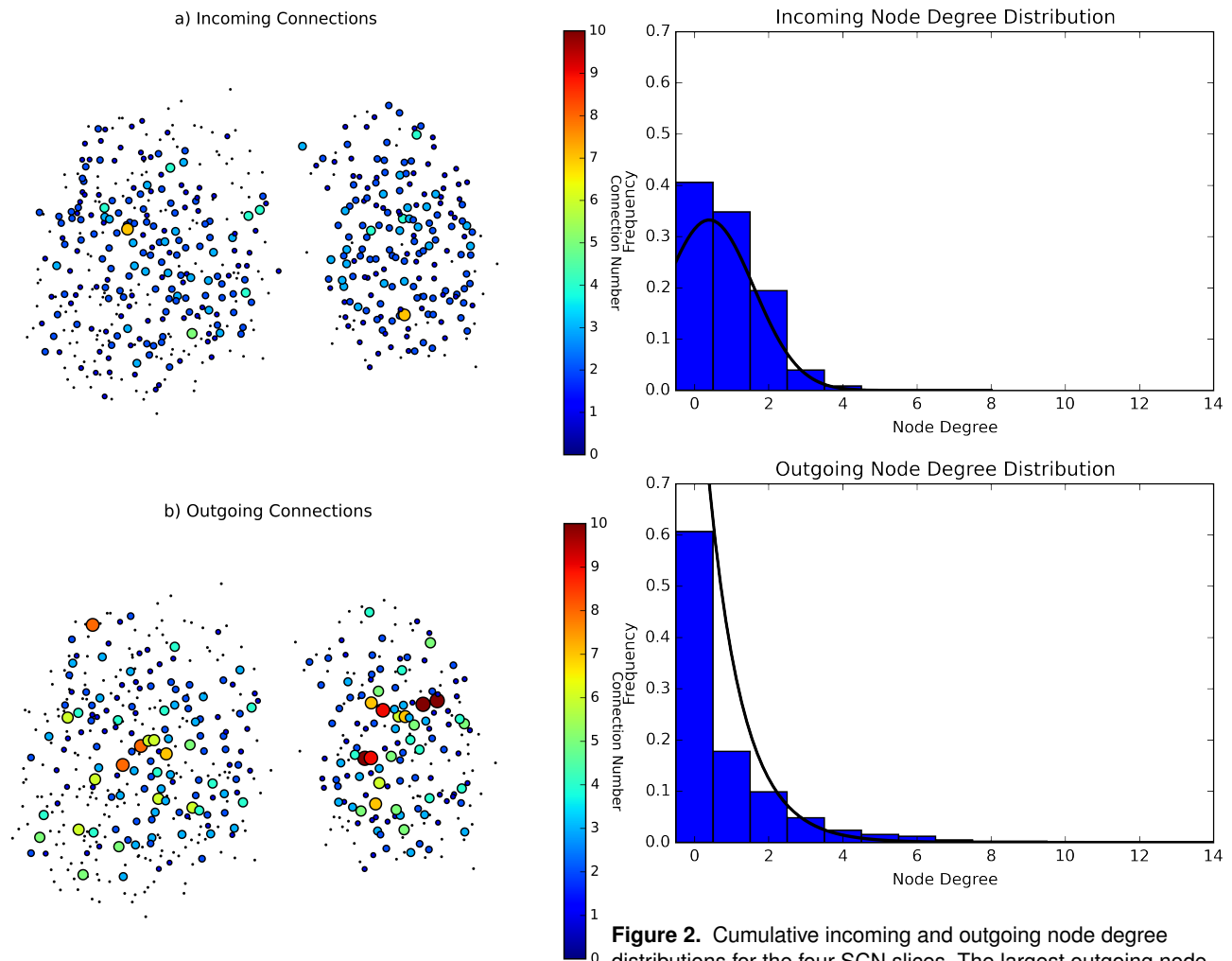


Figure 1. Incoming (a) and outgoing (b) connections for SCN 1. Nodes are sized and colored according to the number of incoming and outgoing connections. The maximum outgoing node degree for this SCN was found to be 10, with node degrees over 5 occurring 20 times ($n = 541$), and the maximum incoming node degree was found to be 7, with node degrees of 5 or more occurring only three times.

of outgoing connections was small world. Approximately 31.3% of those connections were found to be bi-directional, while 68.7% were found to be directed. The neurons with a higher degree of outgoing connections reside preferentially in the core, which would be expected if the core entrains the shell in synchronization [Taylor et al. \(2017\)](#). We suspect that these may be the VIP-ergic neurons as found in [Kalamatianos et al. \(2004\)](#). Simulated networks with this structure result in the highly sparsely connected nodes becoming phase leaders while the more highly connected nodes lag slightly behind. This agrees with the findings of [Taylor et al. \(2017\)](#) that found that core SCN neurons peaked in expression after shell neurons.

The directionality found in this paper resembles the structure of, for example, a corporation. Nearly all nodes have a small number of incoming connections, but select nodes have a much larger number of outgoing connections. This structure suggests that the highly connected nodes drive the resynchronization, while the redundancy of smaller

Figure 2. Cumulative incoming and outgoing node degree distributions for the four SCN slices. The largest outgoing node degree observed was 18, and the largest incoming node degree was 8. Approximately 40% of cells were determined to have no incoming connection and approximately 60% were determined to have no outgoing connection. Of the cells with observed incoming connections, only 1% had more than 3 incoming connections. Of the cells that had observed outgoing connections, 20% had more than 3 outgoing connections.

nodes likely contributes to the robustness of the system. By having a large network with several sparsely connected nodes that exert only a small influence on the overall system, as opposed to a small network in which each node is highly connected and important, random cell death is less likely to disrupt the nodes that drive resynchronization [Abel et al. \(2016\)](#).

Further investigation is necessary to determine the evolutionary benefits such a network structure would confer. Some key questions include whether or not the directed network allows the system to save on the metabolic cost of creating connections while still producing a robust circadian network. Furthermore, it is possible that it also saves on the cost of sending signaling peptides if the system is able to achieve the same level of synchronization with fewer total connections. It is also important to investigate the balance that this structure strikes between being able to adapt to changing external signals on a long time scale such as seasonal lighting changes while maintaining the robustness necessary to minimize short term perturbations such as

lightning strikes and other natural light producing events. We are currently pursuing these directions.

Acknowledgments

This work has been supported by the Institute for Collaborative Biotechnologies through grant W911NF-09-0001 from the U.S. Army Research Office. The content of the information does not necessarily reflect the position or the policy of the Government, and no official endorsement should be inferred.

We would also like to acknowledge Dr. Erik Herzog of Washington University for making the SCN data available to us.

Supplemental materials

Detailed methodology

Inference of phase and amplitude

Conversion of the known PER2 data into a phase and amplitude was performed according to three major steps. The first step was to determine where peaks and troughs occurred. To do this we found the highest PER2 value in the first 28 hours, and set that as the first peak. Next, we chose the lowest PER2 value in the next 20 hours as the subsequent trough. We repeated searching each 20 hour interval for the highest or lowest PER2 value to determine peaks and troughs. Because the first peak found in this way is the first peak at limit-cycle amplitude, we also perform a backwards search. To identify all peaks, the backwards search identifies local maxima that occur prior to the first limit cycle peak, and set the phases of these to $\frac{\pi}{2}$. The reason this may occur multiple times in the first 24 hours is because some cells are still transitioning from a short, free running period to the synchronized circadian period. We note that the time immediately after washout is the most informative in regards to network structure.

Each peak was assigned a phase value of $\frac{\pi}{2}$ and used, together with the relationship

$$\widehat{PER2}(\phi_i(t), A_i(t)) = \frac{A_i(t)}{2} + \frac{A_i(t)}{2} \sin \phi_i(t), \quad (S.1)$$

which is the representation of PER2 in the model, to calculate the corresponding amplitude value. Each trough was assigned a phase value of $\frac{3\pi}{2}$. We then integrated the differential equation model from each peak to the troughs immediately before and after it using the forward Euler method to create initial guesses for the phase and amplitude values for all remaining time points. Because the incoming VIP values were not known at this point, the mean value of possible incoming VIP was used as an approximation. To refine this initial guess, once the amplitude for the trough values was inferred, those were then used as starting points to repeat the integration back to the peaks. This resulted in two sets of phase and amplitude values for each point. These values were averaged according to the number of time steps from a peak or trough (i.e. a point 1 time step away from a peak and 3 steps away from a trough would be weighted with one-quarter the value obtained via the integration that was initialized at the peak and three-quarters

the value obtained via the integration that was initialized at the trough). Finally, optimization of 6 was used to refine the initial estimates. The first term minimizes the difference between the model prediction of PER2 and the observed PER2 values. The second and third terms are regularizations to prevent overfitting. γ_1 , γ_2 and γ_3 are the weights for each term, set at values of 0.6, 0.3, and 0.1, respectively.

Linearization and minimization

Due to the complex series of reactions that make up the core circadian oscillator, the effect of VIP on the phase of the system is non-linear. However, our model uses the concept of a velocity response curve (VRC) to capture these dynamics. The VRC is a curve that represents how the rate of the phase progression of an oscillator will change based on an external signal and is a function of the phase ϕ_i , amplitude A_i , steady state amplitude ss_i and period τ_i of cell i , and K is the base transcription rate. The VRC of rat neurons responding to VIP stimulus has been studied and is an integral part of the phase amplitude model. Using this we linearize the system as follows:

We can rearrange equation 4 to give:

$$\gamma_i(t) = \frac{(\frac{d\phi_i(t)}{dt} - 1) * K}{VRC(\phi_i(t), A_i(t), ss_i, \tau_i) + 1 - \frac{d\phi_i(t)}{dt}}. \quad (S.2)$$

By doing this, and substituting in

$$\gamma_i(t) = \sum_i VIP_{out}(t) * C_i, \quad (S.3)$$

together with the model approximation for VIP released as a function of the amount of PER2 present,

$$VIP_{out,i}(t) = 12 \frac{\widehat{PER2}_i(t)}{4 + \widehat{PER2}_i(t)}, \quad (S.4)$$

we obtain

$$\sum_i 12 \frac{\widehat{PER2}_i(t)}{4 + \widehat{PER2}_i(t)} * C_i = \frac{(\frac{d\phi_i(t)}{dt} - 1) * K}{VRC(\phi_i(t), A_i(t), ss_i, \tau_i) + 1 - \frac{d\phi_i(t)}{dt}}. \quad (S.5)$$

We use the forward Euler method to approximate the derivative $\frac{d\phi_i(t)}{dt}$, yielding

$$\sum_i 12 \frac{\widehat{PER2}_t}{4 + \widehat{PER2}_t} * C_i = \frac{(\frac{\phi_{i,t} - \phi_{i,t_{prev}}}{t - t_{prev}} - 1) * K}{VRC(\phi_i(t), A_i(t), ss_i, \tau_i) + 1 - \frac{\phi_{i,t} - \phi_{i,t_{prev}}}{t - t_{prev}}}. \quad (S.6)$$

Denoting the LHS of equation (S.5) by $VIP_{out} * C_i$ and the RHS by $VIP_{in,i}$ the minimization can be written as

$$\min_{C_i} \sum_i \|VIP_{in,i}(\phi_i(t), A_i(t)) - VIP_{out}(\widehat{PER2}(t)) * C_i\|, \quad (S.7)$$

where VIP_{out} was calculated using the actual PER2 data, and VIP_{in} was found using the model predictions for phase and amplitude. Using this, we implemented the minimization to produce a set of incoming connections for each cell. The minimization was implemented using the `scipy.optimize.least_squares` function for Python (documentation available at https://docs.scipy.org/doc/scipy/reference/generated/scipy.optimize.least_squares.html) with its default parameters, with the solutions constrained between 0 and 1. The default method for solving the least squares problem is the Trust Region Reflective algorithm. Doing this for all cells solves for the incoming and outgoing connections, resulting in a directed connectivity matrix with weights between 0 and 1. If a connection weight was found to be greater than 0.01, that connection was deemed to exist.

Assessment of accuracy

To assess the accuracy of the algorithm we first generated 15 synthetic networks *in silico*. The networks were generated to have an exponentially decaying node degree distribution according to the Circle Network algorithm described in [Vasalou et al. \(2009\)](#). These bidirectional networks had 20 nodes (corresponding to cells) and were initially to have an average node degree of 4. To turn these networks into directed networks for testing, each bidirectional connection was given a one-in-three chance of either remaining bidirectional, or becoming unidirectional in one of the two directions.

The directed networks were then used together with randomly generated initial conditions to produce model PER2 values for each virtual cell based on the phase amplitude model outlined in [Webb et al. \(2012\)](#). Using this synthetic data, the techniques outlined in the "Inference of phase and amplitude" section of the Supplemental materials were then implemented to re-determine the phase and amplitude values for each cell, and the linearization and minimization methods detailed in the Supplemental materials were used to infer the network, beginning with the undirected network.

To test the sensitivity of the algorithm, we ran tests where we perturbed model parameters by 20% when generating the synthetic data to examine the effects this had on the inference accuracy. Additionally, to test the effects of noise on the algorithm, Gaussian noise was added to the data after generation, but before phase and amplitude determination. The standard deviation of the noise applied was sized relative to the average PER2 value of the pre-noise data. The results of these tests are summarized in Table S1. The undirected networks each had 140 possible connections. 15 trials were performed for each test, resulting in 2100 total attempted inferences per test. When inferring the phase and amplitude values, the data was fit to a sine curve to mimic the model. The inference yielded excellent results (ACC = 0.846, SPC = 0.786) even at relatively high levels of Gaussian noise ($\sigma_{noise} = 0.2PER2_{avg}$), as shown in Table S1. It should be noted that the inferred functional networks are still only functional models of the communication network involved in the synchronization of PER2 expression. It is unlikely that they capture all physical connections that exist between neurons. For higher degree incoming nodes ($k_{in} > 4$) the

Table S1. Test Results For Synthetic Network Inference With Noise

Test	TP	FP	TN	FN	ACC	TPR	SPC
$\sigma_{noise} = 0$	89.5	4.8	40.9	4.8	0.931	0.949	0.895
$\sigma_{noise} = 0.1PER2_{avg}$	88.1	5.3	39.5	6.2	0.911	0.934	0.895
$\sigma_{noise} = 0.2PER2_{avg}$	83.5	9.5	34.9	10.8	0.846	0.885	0.786
$\sigma_{noise} = 0.3PER2_{avg}$	82.1	10.0	33.5	12.2	0.826	0.871	0.770
$\sigma_{noise} = 0.4PER2_{avg}$	78.3	13.0	29.7	16.0	0.771	0.830	0.696
$\sigma_{noise} = 0.5PER2_{avg}$	75.3	15.0	26.7	19.0	0.729	0.799	0.640
$\sigma_{noise} = 0.1PER2_{avg}, k_{in} > 4$	64.1	5.6	15.5	30.2	0.690	0.680	0.735
$\hat{\beta} = \beta \cdot 10^1$	65.9	8.7	17.3	28.4	0.594	0.699	0.665
$\hat{\beta} = \beta \cdot 10^{-1}$	70.0	8.9	21.4	24.3	0.653	0.742	0.706

confidence of the method decreases, as expressed in the table, marked most noticeably by an increase in the number of false negatives. This is likely due to the redundancy of some of the inputs.

Experimental methods

Cell culture and bioluminescence recording

The SCNs used in this experiment were taken from homozygous PER2::LUC mice. The mice were 7-d-old and were kept in a 12-h:12-h light:dark cycle environment. All methods comply with guidelines set forth by the National Institutes of Health and were approved by the Washington University Animal Studies Committee. Bilateral SCN from 300- μ m coronal sections of hypothalamus were cultured on Millicell-CM membranes (Millipore) in 400 mL air-buffered DMEM with two full-volume exchanges every 7 d. The culture remained *in vitro* for 14 d and was subsequently moved to the stage of an inverted microscope (Nikon TE2000 fitted with a 20x objective and a 0.5x coupler resulting in a total of 10x magnification) inside a dark incubator (In Vivo Scientific). We then incorporated 0.15 mM beetle luciferin (BioThema) to the medium and imaged bioluminescence at 36C with an ultrasensitive CCD camera (Andor Ixon; 1 x 1 binning, 1-h exposure). 2.5 M TTX (Sigma) was then applied to SCN cultures as described in [26]. After 6 d, we removed the TTX from the medium via three full-volume exchanges of fresh medium. We resumed recording for 8-12 d to monitor resynchronization of PER2::LUC rhythms. After washes, bright field images were used to ensure culture alignment and focus was consistent with prior images.

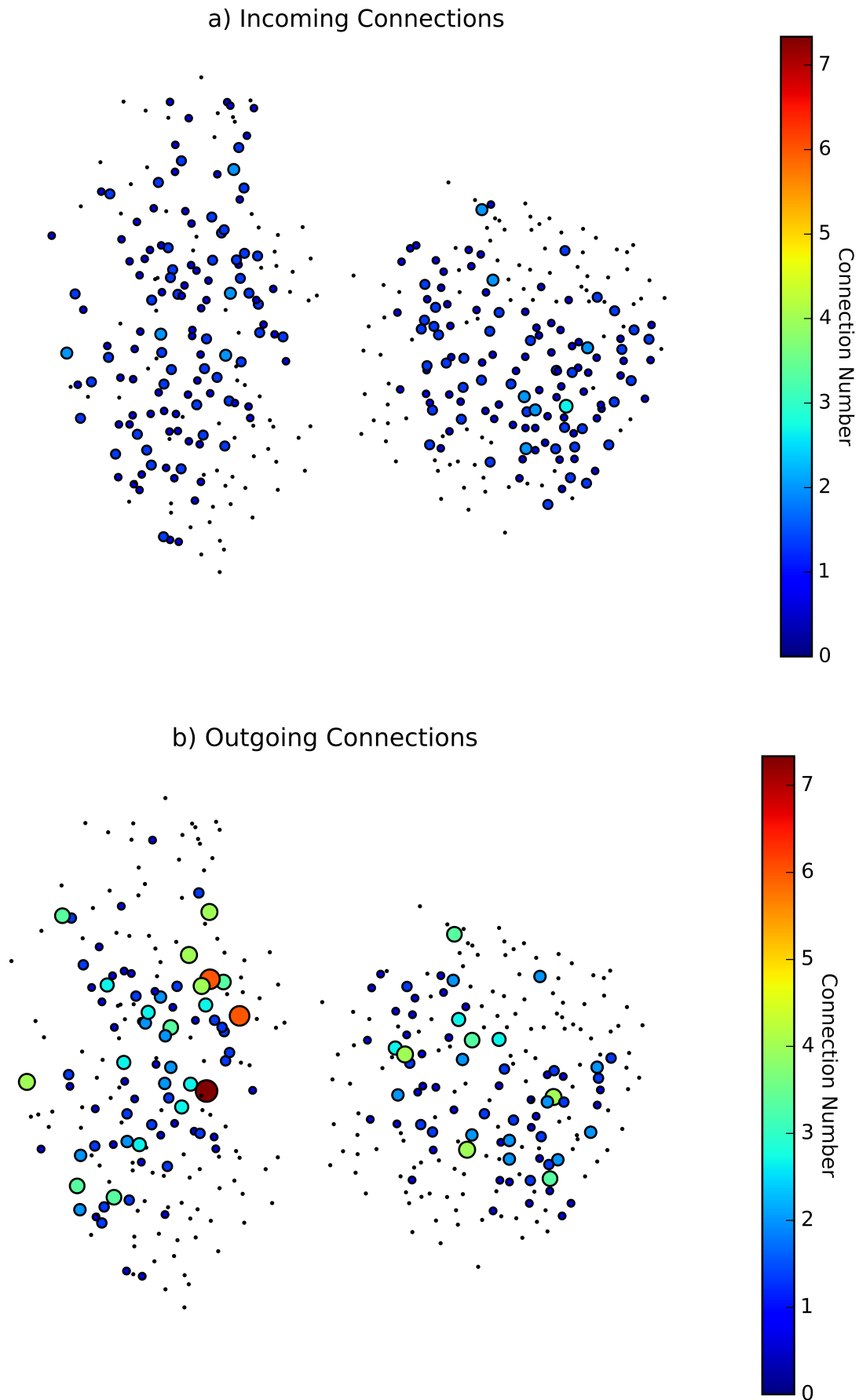


Figure S1. Incoming (a) and outgoing (b) connections for SCN 2. Nodes are sized and colored according to the number of incoming and outgoing connections.

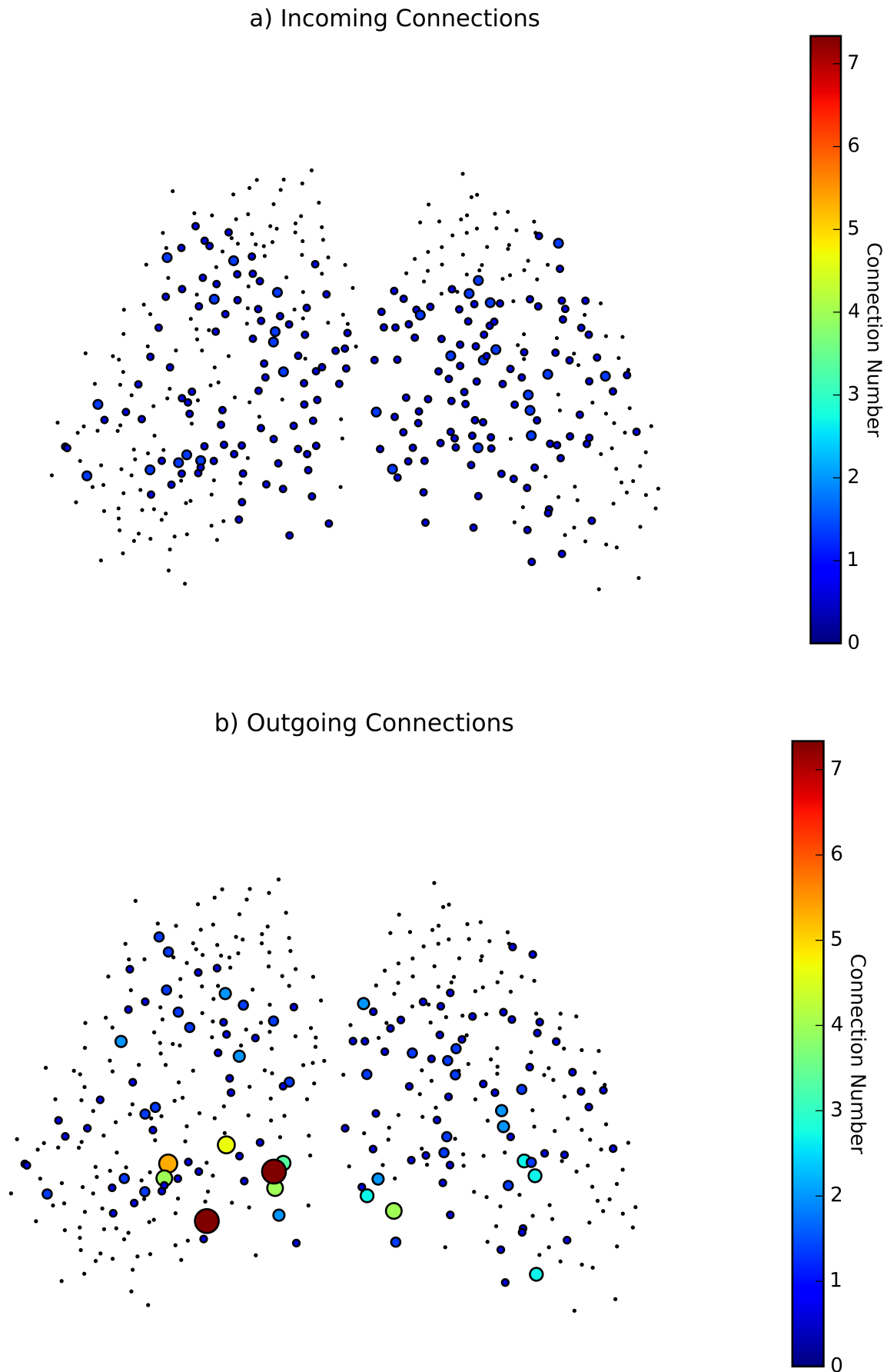


Figure S2. Incoming (a) and outgoing (b) connections for SCN 3. Nodes are sized and colored according to the number of incoming and outgoing connections.

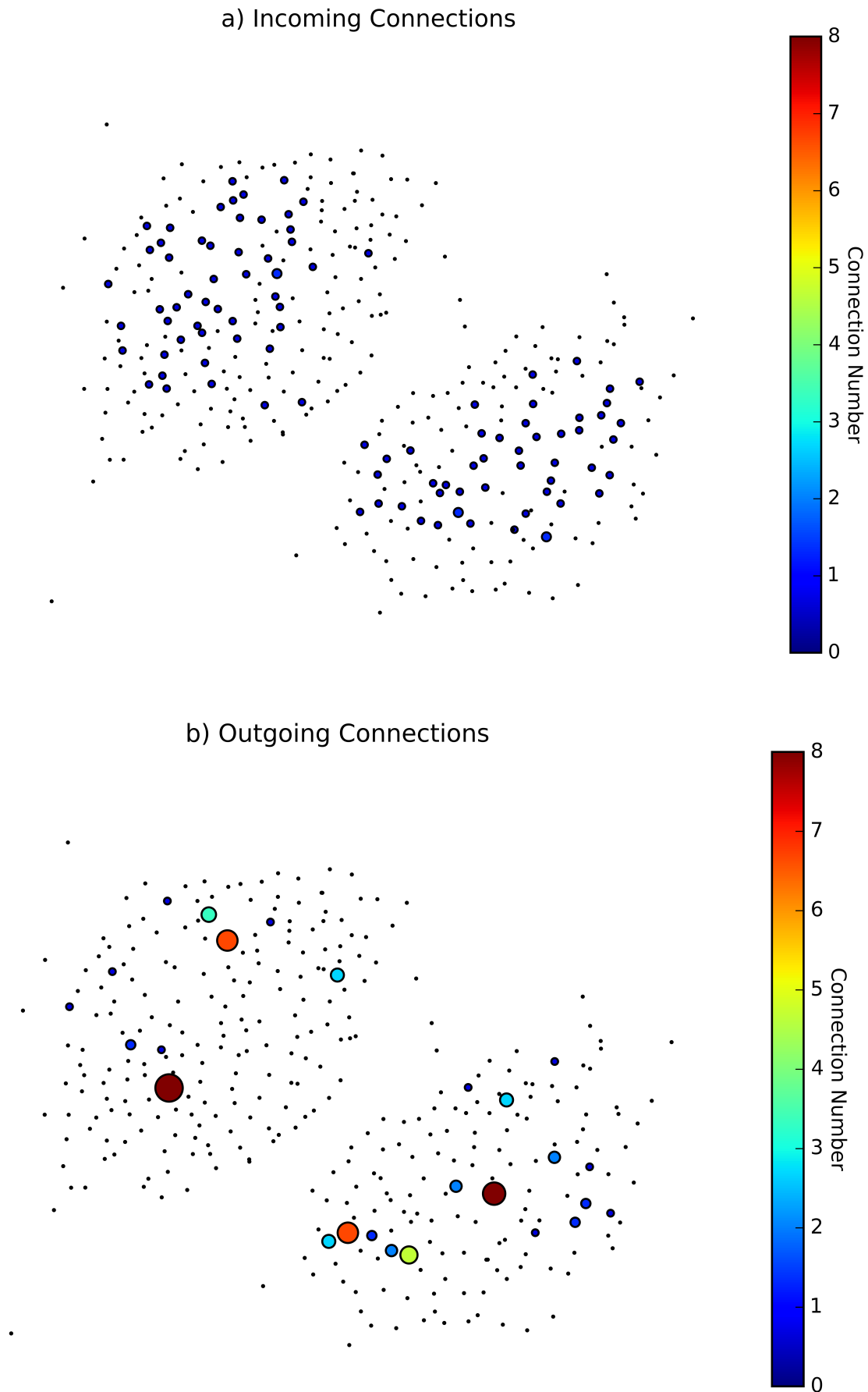


Figure S3. Incoming (a) and outgoing (b) connections for SCN 4. Nodes are sized and colored according to the number of incoming and outgoing connections.

References

- Dunlap JC (1999) Molecular bases for circadian clocks. *Cell* 96: 271290.
- Ralph MR, Foster RG, Davis FC, Menaker M (1990) Transplanted suprachiasmatic nucleus determines circadian period. *Science* 247: 975978.
- Bass J, Takahashi JS (2010) Circadian integration of metabolism and energetics. *Science* 330(6009):13491354.
- Liu AC, Welsh DK, Ko CH, Tran HG, Zhang EE, Priest AA, Buhr ED, Singer O, Meeker K, Verma IM, Doyle FJ III, Takahashi JS, Kay SA (2007) Intercellular coupling confers robustness against mutations in the SCN circadian clock network. *Cell* 129(3): 605616.
- Stelling J, Gilles ED, Doyle FJ III (2004) Robustness properties of circadian clock architectures. *PNAS* 101 (36) 13210-13215.
- Leloup JC, Goldbeter A (2003) Toward a detailed computational model for the mammalian circadian clock. *Proc Natl Acad Sci U S A* 100: 70517056.
- To TL, Henson MA, Herzog ED, Doyle FJ III (2007) A Molecular Model for Intercellular Synchronization in the Mammalian Circadian Clock. *Biophys J* 92: 37923803.
- Aton SJ, Colwell CS, Harmar AJ, Waschek J, Herzog ED (2005) Vasoactive intestinal polypeptide mediates circadian rhythmicity and synchrony in mammalian clock neurons. *Nat Neurosci* 8(4):476483.
- DeWoskin D, Myung J, Belle MD, Piggins HD, Takumi T, Forger DB. (2015) Distinct roles for GABA across multiple timescales in mammalian circadian timekeeping. *Proc Natl Acad Sci USA* 112(29):E3911E3919.
- Cutler DJ, Haraura M, Reed HE, Shen S, Sheward WJ, Morrison CF, Marston HM, Harmar AJ, Piggins HD (2003) The mouse VPAC2 receptor confers suprachiasmatic nuclei cellular rhythmicity and responsiveness to vasoactive intestinal polypeptide in vitro. *Eur. J. Neurosci.* 17:197204.
- Vasalou C, Herzog ED, Henson MA (2009) Small-world network models of intercellular coupling predict enhanced synchronization in the suprachiasmatic nucleus. *J Biol Rhythms* 24(3):243254.
- Gonze D, Bernard S, Waltermann C, Kramer A, Herzog H (2005) Spontaneous synchronization of coupled circadian oscillators. *Biophys J* 89: 120129.
- Abel JH, Meeker K, Granados-Fuentes D, St. John PC, Wang TJ, Bales BB, Doyle FJ III, Herzog ED, and Petzold LR (2016) Functional network inference of the suprachiasmatic nucleus. *PNAS* 2016 113 (16) 4512-4517.
- Abrahamson EE, Moore RY. (2001) Suprachiasmatic nucleus in the mouse: retinal innervation, intrinsic organization and efferent projections. *Brain Res.* 2001;916:172191.
- Welsh DK, Logothetis DE, Meister M, Reppert SM (1995) Individual neurons dissociated from rat suprachiasmatic nucleus express independently phased circadian firing rhythms. *Neuron.* 14:697706.
- Cagampang FR, Sheward WJ, Harmar AJ, Piggins HD, Coen CW. (1998) Circadian changes in the expression of vasoactive intestinal peptide 2 receptor mRNA in the rat suprachiasmatic nuclei. *Brain Res. Mol. Brain Res.* 54:108112.
- Kalamatianos T, Kallo I, Piggins HD, Coen CW (2004) Expression of VIP and/or PACAP receptor mRNA in peptide synthesizing cells within the suprachiasmatic nucleus of the rat and in its efferent target sites. *Journal of Comparative Neurology.* 475:1935.
- Garofalo M, Nieuws T, Massobrio P, Martinoia S (2009) Evaluation of the performance of information theory-based methods and cross-correlation to estimate the functional connectivity in cortical networks. *PLoS One* 4(8):e6482
- Bettencourt LM, Stephens GJ, Ham MI, Gross GW (2007) Functional structure of cortical neuronal networks grown in vitro. *Phys Rev E Stat Nonlin Soft Matter Phys* 75(2 Pt 1):021915.
- Kamiski M, Ding M, Truccolo WA, Bressler SL (2001) Evaluating causal relations in neural systems: Granger causality, directed transfer function and statistical assessment of significance. *Biol Cybern* 85(2):145157
- Pourzanjani A, Herzog ED, Petzold LR (2015) On the Inference of Functional Circadian Networks Using Granger Causality. *PLoS One* 10(9):e0137540
- Fujita KA, Toyoshima Y, Uda S, Ozaki Y, Kubota H, Kuroda S (2010) Decoupling of receptor and downstream signals in the Akt pathway by its low-pass filter characteristics. *Sci Signal* 3(132):ra56
- Webb AB, Taylor SR, Thoroughman KA, Doyle FJ III, Herzog ED (2012) Weakly Circadian Cells Improve Resynchrony. *PLoS Comput Biol* 8(11): e1002787. <https://doi.org/10.1371/journal.pcbi.1002787>
- Taylor SR, Wang TJ, Granados-Fuentes D, Herzog ED (2016) Resynchronization Dynamics Reveal that the Ventral Entrain the Dorsal Suprachiasmatic Nucleus. *Journal of Biological Rhythms* Vol 32, Issue 1, pp. 35 - 47
- Leak RK, Card JP, Moore RY. Suprachiasmatic pacemaker organization analyzed by viral transynaptic transport. *Brain Research.* 819:2332.
- Webb AB, Angelo N, Huettner JE, Herzog ED (2009) Intrinsic, nondeterministic circadian rhythm generation in identified mammalian neurons. *Proc Natl Acad Sci USA* 106(38):1649316498
- Taylor SR, Webb AB, Smith KS, Petzold LR, Doyle FJ III (2010) Velocity response curves support the role of continuous entrainment in circadian clocks. *J Biol Rhythms.* 25(2):138-49
- Abraham U, Granada AE, Westermark PO, Heine M, Kramer A (2010) Coupling governs entrainment range of circadian clocks. *Mol Syst Biol.* 6:438
- Schmal C, Herzog ED, Herzog H (2018) Measuring Relative Coupling Strength in Circadian Systems 33(1): 84-98